Compact And Robust Laser Impulse Measurement Device, With Ultrashort Pulse Laser Ablation Results

Dr. Kevin Kremeyer, Dr. John Lapeyre, Dr. Steven Hamann

Physics, Materials, and Applied Mathematics Research, L.L.C.
PM&AM Research
1665 E. 18th Street, Suite 112
Tucson, AZ, 85719.

Abstract. An impulse measurement device and analysis package was conceived, designed, constructed, tested, and demonstrated to be capable of: measuring nanoNewton-seconds to milliNewton-seconds of impulse due to laser-ablation; being transported as carry-on baggage; set-up and tear-down times of less than an hour; target exchange times of less than two minutes (targets can be ablated at multiple positions for thousands of shots); measurements in air and in vacuum; error of just a few percent; repeatability over a wide range of potential systematic error sources; and time between measurements, including ring-down and analysis, of less than 30 seconds. The instrument consists of a cantilever (i.e. leaf spring), whose time-dependent displacement/oscillation is measured and analyzed to determine the impulse imparted by a laser pulse to a target. These shapes are readily/commercially available, and any target material can be used, provided it can be fashioned in the form of a cantilever, or as a coating/film/tape, suitable for mounting on a cantilever of known geometry. The instrument was calibrated both statically and dynamically, and measurements were performed on brass, steel, and Aluminum, using laser pulses of ~7ns, ~500ps, and ~500fs. The results agree well with those published in the literature, with surface effects, atmosphere, and pre-/post-pulses demonstrating interesting effects and indicating areas for further study. These parameters should be carefully controlled and held constant during a series of measurements. The impulse imparted by ablation due to laser filaments in air was also explored.

Keywords: Laser Ablation; Ultrashort Pulse; Impulse Measurement; Space Propulsion; Beamed Energy; Laser Filaments; Atmospheric Propulsion; Shock Dynamics; Fluid Dynamics; Gas Heating.
PACS: 06.30.Ft; 06.30.Gv; 06.60.Mr; 07.10.Pz; 07.35.+k; 07.87.+v; 42.62.Cf; 42.65.Re; 43.; 43.40.+s; 45.20.df; 46.40.-f; 46.80.+j; 47.40.-x; 47.40.Rs; 47.54.Jk; 52.35.Tc; 52.38.Hb; 52.38.Mf; 52.75.Di; 81.65.Lp; 81.70.Bt; 81.70.Cv; 89.20.Bb; 46.70.De;

THRUST STAND DESIGN/OPTIONS:

A number of different "thrust stand" geometries were explored, including low-friction translators and harmonic oscillators. The low-friction translators were quickly rejected because of concerns involving static friction or repositioning the target/system for multiple repeatable measurements/shots. This left a number of harmonic oscillators, including 2-point and 4-point pendulae, steel coil springs, rubber springs, and a leaf-spring (**FIGURE 1**).

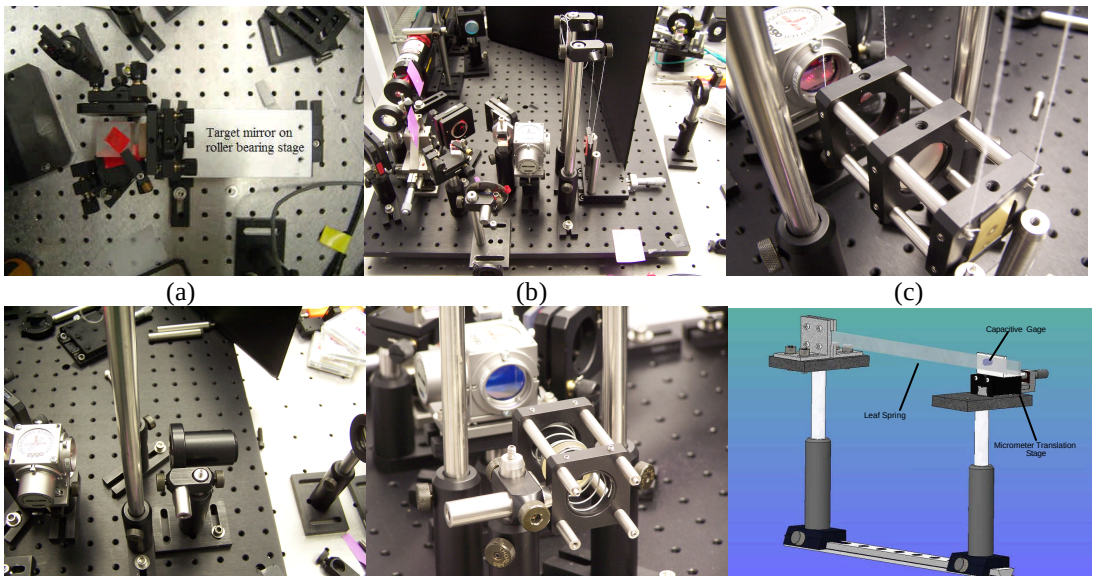

(a) (b) (c)

(d) (e) (f)

FIGURE 1: (a) Interferometric measurement geometries of a: roller bearing stage. (b); 2-point pendulum. (c) 4-point pendulum. (d) O-ring system. (e) Double coil spring system. (f) Schematic of our preferred cantilever/beam.

Each of these choices has some contribution to its motion by modes other than the fundamental spring mode (these include torsional, rotational, and harmonic modes, as well as anharmonicity/nonlinearity from other sources). Through measurement with an interferometer system, we determined that the cantilever (to which we will often refer as a "leaf spring") has the most easily-interpreted oscillation with the best-contained modal excitations. The final design was selected to maximize measurement capabilities and possible geometries, while minimizing the degrees of freedom, thereby allowing simplified system calibration and adaptation. Examples of this versatility include the ability to use thinner or thicker leaf springs, allowing the system displacement to remain relatively constant when different magnitudes of impulse are imparted. In addition to thickness changes, the leaf spring material and length is another source of geometrical flexibility. In the measurement geometries, it was important to know the length of the spring (L), and the position x_a, at which the laser pulse is applied. A further benefit is that these simple targets can be easily fabricated or very economically purchased from a large number of commercial suppliers.

SYSTEM CHARACTERIZATION

The basic concept behind the instrument is that a harmonic oscillator is set into motion when a laser imparts an impulse to it. From measuring the time-dependent oscillation, the impulse can be determined. Historically, practitioners have measured the fundamental mode of a given oscillator to determine the momentum imparted to the oscillator (typically a linear or torsional pendulum). In characterizing the various candidate systems, we established that the extremely sharp impulse delivered by laser pulses excites far more modes than simply the fundamental mode. In the linear (hanging) pendulae, these modes include twisting and vibrations in the target plate. In

torsional pendulae, they include higher-order oscillations in the ixcited arm, as well as vibrations in the target plate. These high-frequency modes typically damp quickly, and do not necessarily cascade their energy (momentum) content inot the fundamental mode. The very high frequencies call for yet higher sampling rates to quantitatively characterize the energy (momentum) contained in them. This also requires a highly accurate model of the different oscillatory modes and their respective phase differences. We selected our final system because of its adherence to a awell-understood 1-D system, whose modes are fully contained in the leaf spring. Even in this simple system, the higher-mode oscillations carry up to 15-25% of the momentum delivered to the target. Selecting the geometry to ensure amplitudes of less than 50 μm, and measuring all of the modes immediately after excitation, has allowed us to quantitatively account for all of the imparted momentum before it is dissipated through any mechanisms. Amplitudes one to two orders of magnitude still fall well within the linear regime for typical configurations.

Optical Interferometry to Benchmark Candidate Measurement Techniques

Our benchmarking interferometer allowed measurement of the displacement and velocity of a target with high precision after a thrust event. A He-Ne Laser was employed to measure displacements to a precision of better than a tenth of a cycle, corresponding to 15.8nm in our double pass interferometer. These measurements allowed an impulse resolution of less than 10 nNs precision, depending on the oscillator's inertial properties/mass. This interferometric approach was used to benchmark and validate the motion of all of the oscillators we considered and to verify performance of various displacement-metrology systems.

Analysis and Calibration:

Our impulse analysis is based on the theory of oscillations in a 1-D system, governed solely by the system dimensions, density, fundamental frequency, and initial conditions. The theory very accurately reproduces higher modes and wave forms that can otherwise look like noise. **FIGURE 2** indicates the remarkably high precision we have been able to achieve with this fundamental approach. The number of modes excited in the physical system is typically determined by the size of the laser spot.

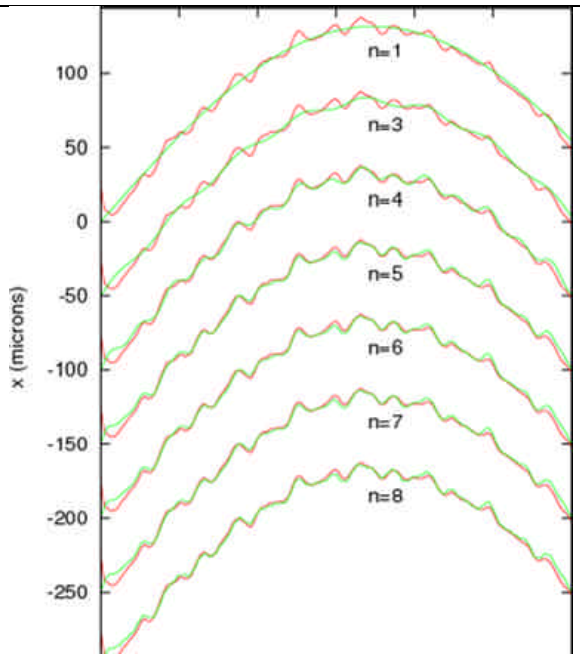

FIGURE 2: Amplitude of a steel spring excited by a laser pulse, compared to theory. The same experimental curve is compared to the theoretical curve obtained by adding increasing numbers of modes (from 1-8). No contribution is given for mode n=2, because the spring was struck at the node for this mode. The agreement is excellent, and the theory requires only measurements as input.

Varying Measurement Position

In addition to varying the spring material/length/thickness and ablation position, we also performed experiments to study the effect on our impulse determination when only the measurement position (fiber optic probe position) was allowed to vary. Geometrical factors and other variables, such as, target preparation, ablation position and spring characteristics were effectively held constant. The main result of this study is that the impulse estimate is independent of measurement position over a wide range, when correctly measured and included in the analysis.

We computed impulse estimates from seventeen ablation shots at nine measurement positions. (Additional positioning shots were made.) The measurement positions varied in fractional position from 0.56 to 0.94 (fractional position is the distance from clamp to tip normalized by the total distance x_a/L.).

The ablation position remained fixed (at fractional position approximately 0.79) for each shot, and a fresh steel tape target was replaced at the point of ablation to ensure an undamaged surface each time. The targets were approximately square with edges approximately 3-5mm long. The measured dynamics were recorded and analyzed to produce impulse estimates with a resulting mean impulse of 6.91 μN-s and an rms deviation of 0.29 μN-s. The relative error computed with the rms is then 4.1%. This relatively high error resulted from the presence of the steel tape, which altered the amplitude of the highest modes from that predicted by the model. Similar measurement series were performed without a steel tape target (simply ablating the same spot on the spring) yielding roughly 2% error, and the range of ablation positions

was also varied, while measuring in the same position, also demonstrating less than 4% error. The range of the spring, over which this low error is generally preserved, is roughly 0.6=f=0.95.

In **FIGURE 3**, we see the time series of two ablation shots measured at the extremes of our range of measurement position. In these plots, f is the fractional measurement position. Although the amplitudes vary by more than a factor of two, the impulse estimated by the theory/model is nearly identical (as it should be). In addition to yet further confirming our confidence in the model, this flexibility in ablation and measurement position relaxes the geometrical constraints, allowing us to choose the geometries most convenient for a given experiment.

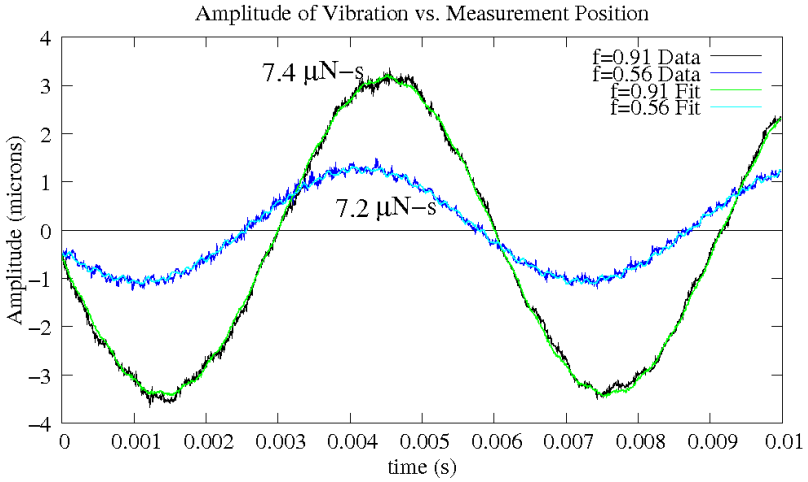

FIGURE 3: Time series of the spring displacement measurement at two different positions. The parameters are the same for the two events, except for the fractional measurement position f. The amplitudes and shapes of the oscillations differ, but the theory/model predicts nearly the same impulse. Note that the model does not correctly predict the highest modes, due to the presence of the small steel tape target mounted on the spring.

Static and Dynamic Calibration

In addition to calculating the impulse from fundamental parameters of the spring itself, we wanted to corroborate these values with independent measures. **FIGURE 4** shows a static calibration of the system, demonstrating the linearity of the system for amplitudes 100 times greater than those used in our measurements. It also demonstrated the accuracy of our "spring constant" (bulk modulus) characterization from the system's fundamental frequency.

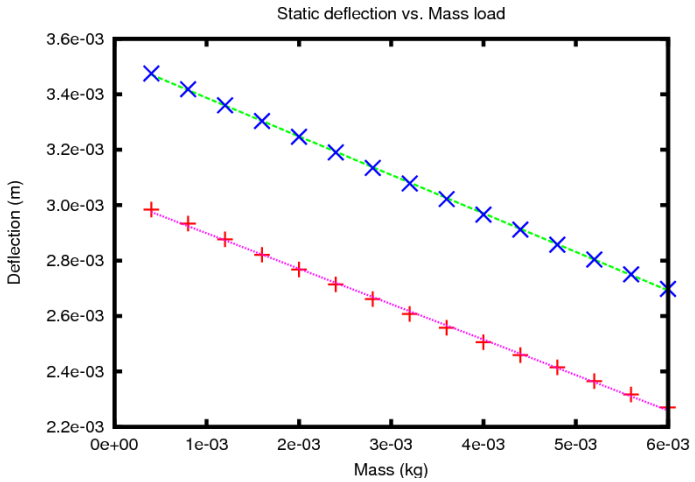

FIGURE 4: Two measurement series, demonstrating the linear response of a typical spring, closely corroborating our dynamic calibration of the "spring constant".

Taking advantage of the above static calibration, we constructed an electromagnet (**FIGURE 5**) and calibrated the static force exerted on the system for a given current. Delivering a known current profile, therefore, resulted in a known impulse being delivered to the system, and this technique allowed us to yet further calibrate our system against a known impulse. The dynamics imparted by the known electromagnetic impulses were very accurately predicted by the model, yielding smoother curves than the typical laser-ablation curves. This resulted from fewer modes being excited by the spatially and temporally more extended distribution of the electromagnetic impulse delivery, compared to that of a laser pulse.

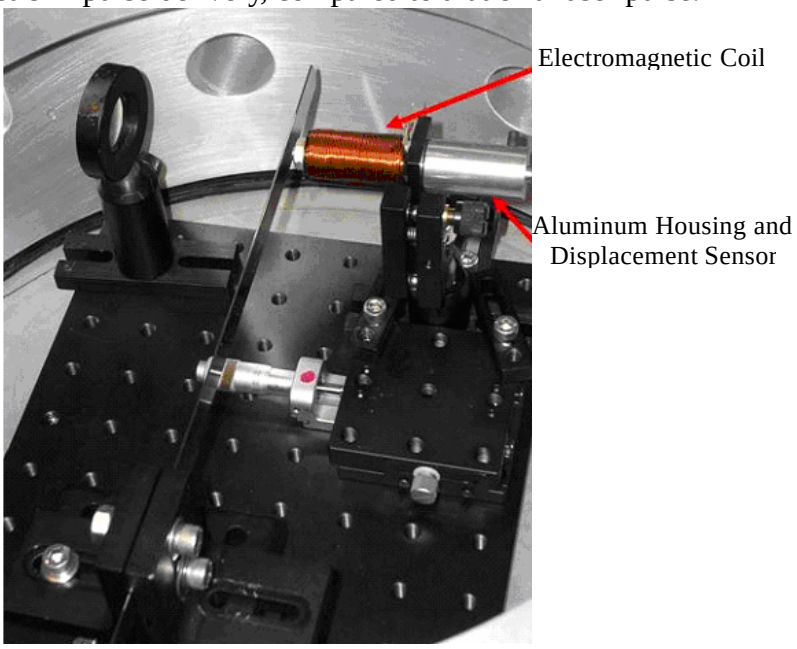

FIGURE 5: Photograph of the calibration coil and target/spring geometry.

The hardware is shown inside of a vacuum chamber at PM&AM Research in **FIGURE 5**. The system is extremely compact and can be transported in carry-on luggage.

Varying Spring Material

There are a number of reasons we want to vary the spring material (i.e. to use springs made of brass, aluminum, or steel). One reason to do this is to eliminate the concern of effects when using a particular material that may introduce error in the measurement. If a wide range of materials (spanning different materials properties, such as density and bulk modulus) is tested to yield similar quantitative results, this indicates the absence of material-specific errors in our model and analysis package.

Another reason to test different materials is that for different experiments, the spring itself may be used as the target. When performing tests to develop the instrument, using the spring as a target is much more efficient than mounting or coating a target material onto the spring. In addition, one may want a softer or stiffer spring in order to tune the sensitivity or response of the instrument. We have performed initial studies indicating that the impulse determination is invariant when using a spring made of steel, aluminum, or brass (these were the materials available to us). **Table 1** shows the results of a single ablation shot applied to each of three springs, each fitted with a small steel target (steel tape). This small steel target ensured that the actual ablated material was the same for the different shots, allowing us to compare the oscillations unique to the different material springs. Most geometric parameters were held fixed as closely as possible, varying primarily thickness (***h***) and material type. We note that the thicknesses, densities and bulk modulii, and thus vibrational frequencies, of these springs/materials vary greatly. Despite this, when fitted with the theory, the results yield nearly identical impulses. After the initial variability that exists during the first 3 shots on a small steel target, we have consistently observed deviations in impulse readings of no more than 2-3% over hundreds of shots thereafter.

TABLE 1: Impulses determined from springs of different materials. Impulse is in μN-s. Distances are in mm, including spring length L, ablation position x_a, and spring thickness h.

Material	***L***	x_a	***h***	***Impulse***
Steel	130	111.0	1.016	5.1
Aluminum	132	111.5	0.52	5.1
Brass	130	111.5	0.813	5.3

IMPULSE MEASUREMENTS

After having characterized our system, we proceeded to take measurements: exploring surface effects; comparing our results to those in the literature; and exploring the impulse imparted by laser filaments.

Surface Effects

The role of surface effects and surface preparation/pre-treatment was demonstrated in the measurements shown in **FIGURE 6**.

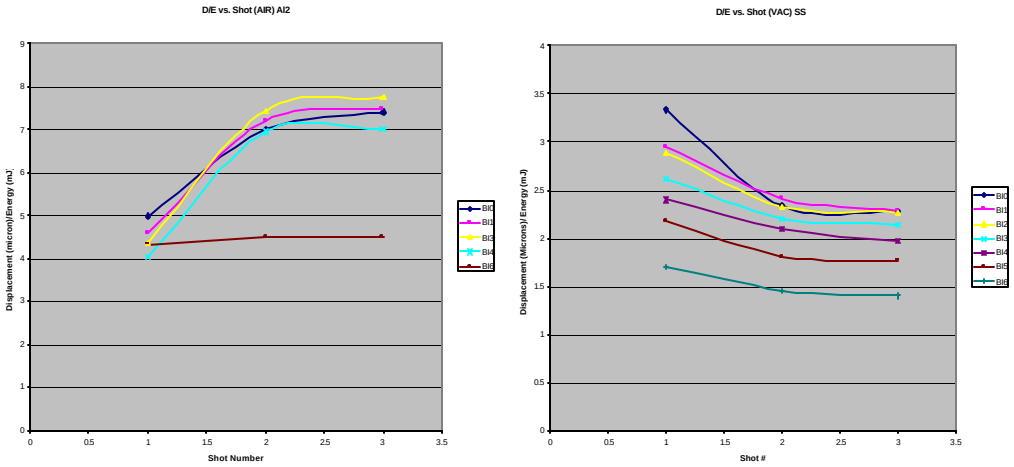

(a) (b)

FIGURE 6: Coupling constants for three successive laser pulses on a given target. Left: Aluminum ablated in air. Right: Stainless steel ablated in vacuum.

In **FIGURE 6**, three successive impulse measurements were taken at several different "pulse energy levels". These pulse energy levels were determined by the laser amplifier settings, which were set for anywhere between very high pulse energies and very low pulse energies. After adjusting the amplifier settings, an unadulterated target surface was targeted, and three shots were then delivered to this same target position, recording the impulse delivered by each, and dividing by the actual laser pulse energy to obtain the coupling constant. The coupling constant measurement from the first pulse at a given energy level is shown as the left-most data point of each line. The coupling constant from the second pulse is shown as the central data point in a given line. Lastly, the coupling constant from the third pulse is shown as the right-most data point of each line. For Aluminum ablated in air, impulse is least efficiently generated during the first shot (on the virgin surface) and the efficiency (coupling) increases dramatically for the ensuing pulses. This effect is negligible near the ablation threshold. For stainless steel ablated under vacuum, impulse is most efficiently generated during the first shot (on the virgin surface), with the efficiency decreasing during the ensuing pulses. The effect is again weakest at the smallest pulse intensities.

Corroboration with Results in the Literature

In the literature, it is common to characterize a system in terms of the fluence that gives the maximum thrust per unit energy. This fluence depends on both the target material (the propellant) as well as the laser parameters. We determined this "optimal fluence" Φ_{opt} for steel and aluminum for 500fs pulses by measuring the coupling coefficient. This determination served both as a test of the instrument, as well as a test of the recent projection by Phipps et al. [2] of how the most efficient fluence depends

on laser pulse length. Measurements using 500fs pulses have not previously appeared in the literature. Our results agree roughly with the predictions of Phipps et. al.[2].

Figure 7 shows coupling coefficient vs fluence for ablation of steel with 500 fs pulses. One curve represents shots on the virgin steel surface (as delivered by the manufacturer). The other curve represents the second shot, following ablation by the first. It is clear that the properties of the surface affect the coupling constant (underscoring the importance of surface effects shown in **Figure 6**). The optimal coupling fluence Φ_{opt} is roughly the same for both curves in **Figure 7**. We note that the value $\Phi_{opt} \sim 1.2 - 1.4 \times 10^4$ agrees well with the prediction of Phipps et al for 500 fs pulses (**Figure 11**).

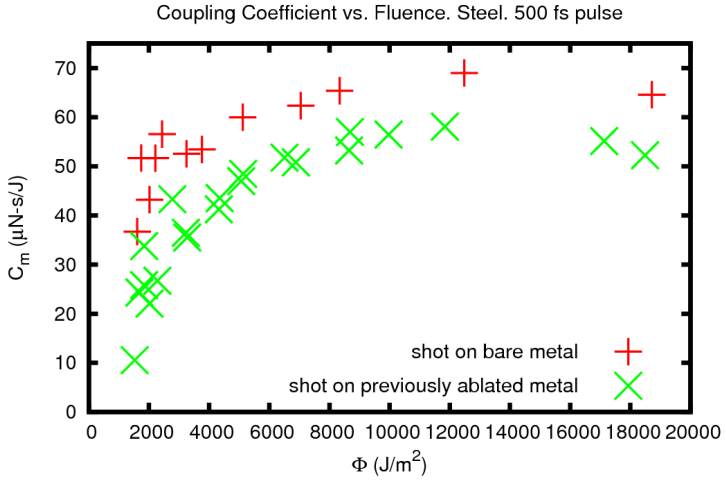

FIGURE 7: C_m as a function of fluence for ablation of steel with 500fs pulses in vacuum.

To explore yet another often uncontrolled parameter in ablation investigations, a study was performed using 500fs pulses, recording the tuning of the seed laser to keep track of the presence of a pre- or post-pulse. **FIGURE 8** shows our measurement of coupling constant vs. fluence for aluminum ablated with a 500 fs laser pulse at 1054nm. From the plot, we determined that the peak coupling coefficient occurs at a fluence of ~4000 Joules/m^2. The strong effect of pre-pulse vs. post-pulse is seen on the efficiency of generating impulse (i.e. in the coupling constant).

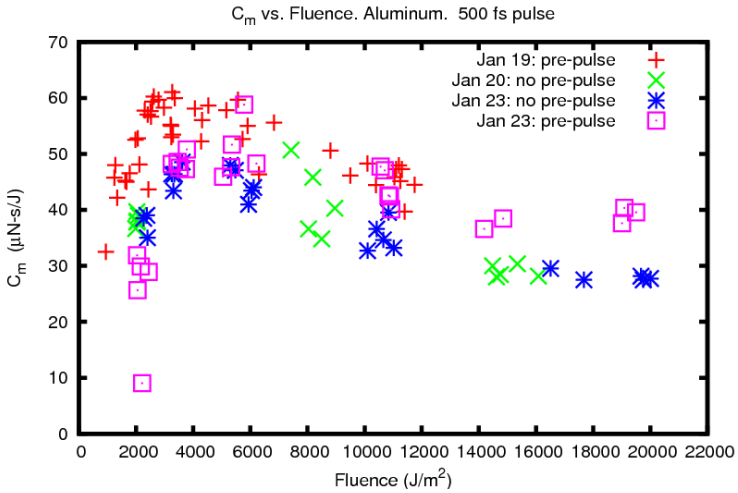

FIGURE 8: C_m as a function of fluence for ablation of Aluminum with 500fs pulses in vacuum.

In figure 8, although certain groups of data points have more or less of their energy in the form of a pre-pulse, the entire data set provides a rough indication of the optimal coupling fluence Φ_{opt}. The predicted value did not agree fully with the predictions of Phipps (**FIGURE 11**), prompting us to perform another study, in which the laser seed configuration remained constant, and the fluence was adjusted by adjusting the laser spot size on the target. These results are shown in **FIGURE 9**, and the measured value of Φ_{opt} is the same as that measured from the data set in **Figure 8** to within the calculated error bars (the size of the data points shown in **Figure 11**). This gave us yet further confidence in our measurement system and analysis model. **FIGURE 9** shows the data for Al and 500 fs pulses organized by spot size.

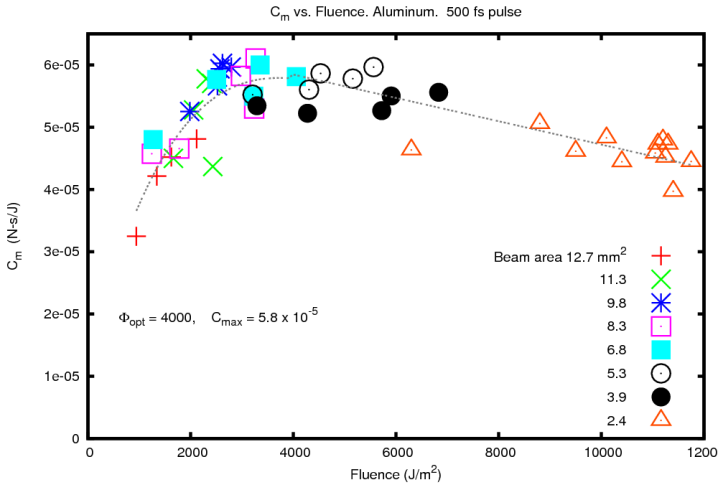

FIGURE 9 C_m as a function of fluence for ablation of Aluminum with 500fs pulses in vacuum. In this graph, the data points are grouped in terms of the spot-size

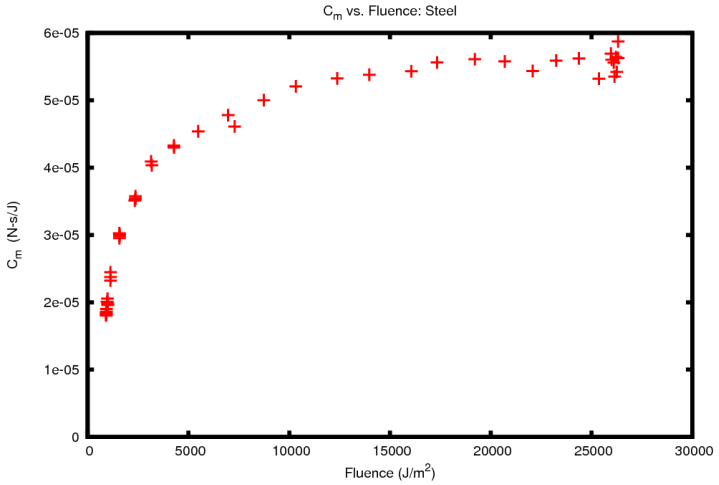

FIGURE 10 C_m as a function of fluence for ablation of steel with 7 ns pulses in air.

FIGURE 10 shows C_m vs. fluence for ablation of steel with 7 ns pulses in air. The plot shows a maximum C_m of about 55 microN-s/J at a fluence of about 2 x 10^5 J/m^2. This Φ_{opt} value is measured in air (upper triangle on the plot from Phipps), as opposed to in vacuum, as are the other points on Phipps's plot (**FIGURE 11**). It is roughly four

times higher than the middle of an expected median value (lower triangle) (indicating that a lower value of Φ_{opt} would be measured in vacuum).

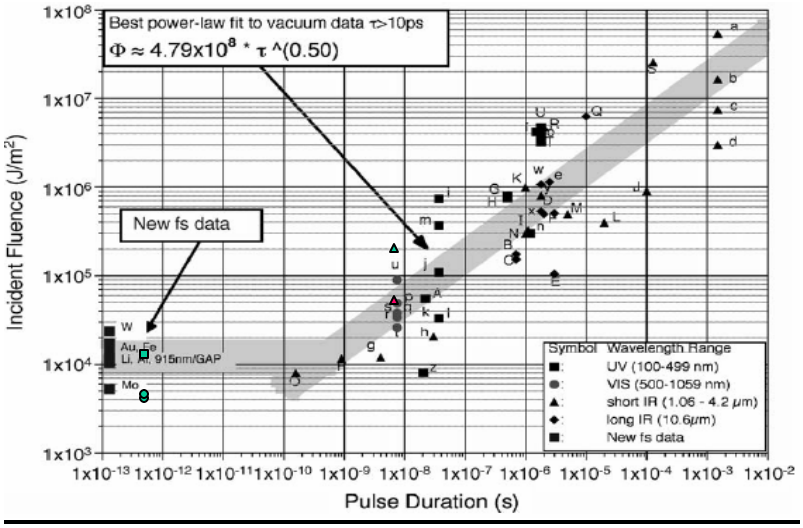

FIGURE 11: Our 1064nm, 500fs data for Al (circles) and Steel (square), overlaid on data from Phipps et al. Our 1064nm, 7ns Steel ablated in air (top triangle) is also shown with a Φ_{opt} four times larger than that anticipated for the impulse in vacuum (bottom triangle).

Impulse Imparted by Ultrashort Pulse Laser Filaments

In another set of experiments, we examined the effect of filaments on the coupling coefficient. We allowed one or more filaments to form spontaneously from propagation of the laser pulse over a few meters with a very slight convergent focus. The filaments occupied a very small fraction of the total cross-section of the pulse, but have a fluence that is significantly higher than the remainder of the pulse (with the difference depending on pulse parameters).

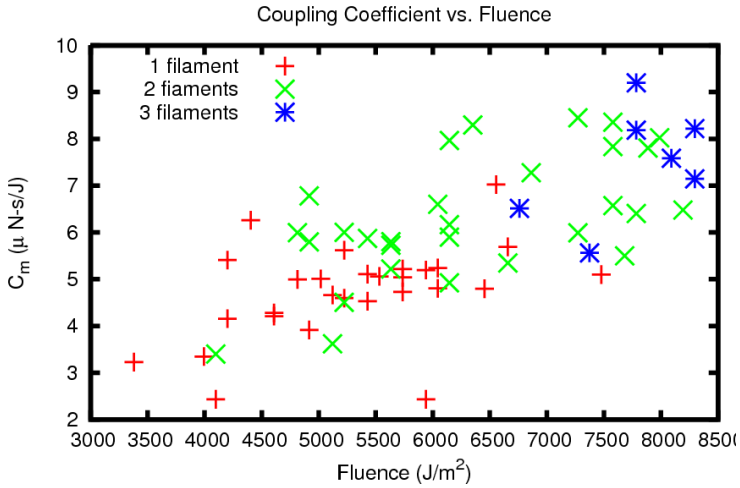

FIGURE 12: Coupling Coefficient as a function of average fluence of a laser spot which has 1-3 filaments formed when it ablates the target.

In **FIGURE 12** we show C_m vs. fluence for pulses containing one, two, or three filaments, in which it can be seen that the number of filaments increases with fluence (we kept a constant spot size in this set of experiments). The plot also shows that in the fluence regimes dominated by a given number of filaments, the maximum coupling constant is enjoyed by the pulses exhibiting the dominant number of filaments. In other words, in the fluence range over which 2 filaments occur most frequently, the maximum coupling constant is also demonstrated by 2 filaments. This is similarly demonstrated in the fluence ranges dominated by 1 and 3 filament shots. This relationship is unclear in the transitional area between the regions of 1 and 2 filaments and between the regions of 2 and 3 filaments. The final conclusion is that in the regime in which filaments form, the number of filaments in a pulse tends to adjust itself to achieve the maximum coupling constant among the choices. In general, the filamenting pulses converted laser energy to momentum less efficiently than non-filamenting pulses, however, their ability to propagate over very long distances without diffraction/spatial spreading can be of great operational utility.

CONCLUSION:

We have designed, built, and characterized a compact and rugged laser-impulse measurement device, capable of measuring nanoNewton-seconds to milliNewton-seconds. The measured impulse values carry an RMS error of ~4% or less, and the system has been designed for extremely fast, simple, and reliable set-up, tear-down, and data-acquisition. The results agree well with those already published in the literature. Atmosphere, surface state, and pre-/post-pulse must be held constant in a series of measurements. Their effects and the impulse imparted by laser filaments have been identified as areas for further study.

REFERENCES

1. Z. Y. Zheng, J. Zhang, Z. Q. Hao, Z. Zhang, M. Chen, X. Lu, Z. H. Wang, and Z. Y. Wei, OPTICS EXPRESS 1061626 **Vol. 13**, No. 26 (December 2005).
2. C. Phipps, J. Luke, D. Funk, D. Moore, J. Glownia, T. Lippert, Applied Surface Science **252,** 4838–4844 (2006)
3. B. C. D'Souza and A. D. Ketsdever, 36th AIAA Plasmadynamics and Lasers Conference AIAA-2005-5172, (6-9 June 2005).